IET Generation, Transmission & Distribution

Research Article

IET Journals
The Institution of Engineering and Technology

Mitigation of transient overvoltages in microgrid including PV arrays

ISSN 1751-8687
Received on 4th July 2019
Revised 25th December 2019
Accepted on 27th April 2020
E-First on 9th June 2020
doi: 10.1049/iet-gtd.2019.1035
www.ietdl.org

Eman Ahmed Awad[1], Ebrahim A. Badran[1] ✉

[1]*Electric Engineering Department, Faculty of Engineering, Mansoura University, Egypt*

✉ *E-mail: ebadran@mans.edu.eg*

Abstract: This study investigates the mitigation of transient overvoltages (TOVs) in a microgrid supplied by renewable distributed generation resources, which include photovoltaic (PV) generators, hydro generation unit, and wind power generators. ATP/EMTP is used in this study as electromagnetic transient software. Accurate simulation models are needed to carry out the study. Therefore, a three-phase PV system model based on the equivalent Newton–Raphson circuit is used, and the efficiency of the PV system components is studied. Then, the use of the PV generation system model for switching studies is investigated using two different electrical systems. The use of different mitigation methods for TOVs at the microgrid is investigated. Three different mitigation methods are considered. First, a device to compensate reactive power such as static var compensator (SVC) is represented as a TOVs mitigation method. Then, adding a supercapacitor as TOVs mitigation method is evaluated. After that, a combination of active and reactive power simultaneously to mitigate TOV, by the addition of SVC to a supercapacitor, is investigated. The grid-connected mode and isolated mode of the microgrid are considered. The results show that the usage of SVC with supercapacitor has the ability to mitigate the transient overvoltage and the waveforms are more regular.

1 Introduction

Solar microgrid (μG) systems can be integrated into other renewable distributed generation resources (RDGRs) such as wind turbines (WTs) or micro-hydro generators. By combining more than one RDGR, the reliability of the μG system can be assured with the generated power available during the year or any weather condition [1, 2]. However, the relatively long computing time required to solve the set of differential equations representing the photovoltaic (PV) generator behaviour causes some problems [3–5].

The linearisation of the PV generator *I*–*V* output characteristic non-linear equation represents the solution to overcome the relatively long computing time required to solve the set of differential equations representing the PV generator behaviour causes some problems [4, 6]. The linearised equivalent electrical circuit is called 'equivalent Newton–Raphson circuit' (ENRC) of a PV generator [6].

In electromagnetic transient software packages and circuit simulators such as ATP/EMTP, a DC source is used instead of a PV generator since there is no such a component embedded in the programme [7, 8]. Using ATP/EMTP, transient analysis of control systems (TACS) is more suitable for models have lower data processing time because it has all the control functions predefined in a feasible environment for the realisation of mathematical routines [8].

Supercapacitors are among the promising technologies, which are attractive for many regenerative applications. Higher power density, faster dynamic response, and longer cycle life are some of the main merits of the energy storage. However, since the supercapacitors have a quick response time, they susceptible to generate high-frequency disturbances in the system [9].

Static var compensators (SVCs) can be installed to solve power quality problems such as a low-power factor, harmonic current pollution, unbalanced problems, and overvoltages. In practical applications, SVCs suffer from the potential resonance problem due to system frequency variation; inductor and capacitor values change, non-linear dynamics characteristics in SVC components such as the thyristors [10].

Recently, many kinds of literature introduce active or/and reactive power compensation devices such as flexible alternating current transmission systems (FACTS) such as SVC and supercapacitors, respectively, to mitigate the problems arises at the power systems [11–15].

This study investigates the mitigation of transient overvoltages (TOVs) in a μG supplied by RDGRs, which includes PV generators, a hydro generation unit (HGU), and wind power generators (WPGs). ATP/EMTP is used in this study as electromagnetic transient software. Accurate simulation models are needed to carry out the study. Therefore, a three-phase PV system model based on ENRC is used, and the efficiency of the PV system components is studied. Then, the use of the PV system model for switching studies is investigated using two different electrical systems.

The use of different mitigation methods for TOVs at the μG is investigated. Three different mitigation methods are considered. First, a device to compensate reactive power such as SVC is represented as a TOVs mitigation method. Then, adding a supercapacitor as TOVs mitigation method is evaluated. After that, a combination of active and reactive power simultaneously to mitigate TOV, by the addition of SVC to a supercapacitor, is investigated. The μG works on two operating modes, connected network mode and isolated mode.

2 Description and modelling of the PV generation unit

2.1 Modelling of the PV generation unit

Fig. 1 shows the difference between the common used the single-diode PV generator model and the ENRC model. The common PV generator model, shown in Fig. 1*a*, consists of a photocurrent source, a non-linear diode, series resistance R_s, which represents the internal losses and shunt resistance, R_{sh} in parallel with diode to take into account leakage current to the ground [4].

A current source and a linear resistance, in parallel with each other, are the elements that represented the ENRC model of the PV generator [4, 6].

The equivalent circuit current of the PV generator model (I_{pv}) is expressed as a function of the PV generator's voltage (V_{pv}) [6]

$$I_{pv} = I_{sc}[1 - K_1(\exp(K_2 V_{pv}^m) - 1)] \quad (1)$$

where the coefficients K_1, K_2, K_3, and K_4, and m are defined as

$$K_1 = 0.01175 \quad (2)$$

$$K_2 = \frac{K_4}{V_{oc}^m} \quad (3)$$

$$K_3 = \ln\left[\frac{I_{sc}(1 + K_1) - I_{mpp}}{K_1 I_{sc}}\right] \quad (4)$$

$$K_4 = \ln\left(\frac{1 + K_1}{K_1}\right) \quad (5)$$

$$m = \frac{\ln(K_3/K_4)}{\ln(V_{mpp}/V_{OC})} \quad (6)$$

where V_{mpp} is the maximum power point voltage, V_{oc} is the open-circuit voltage, I_{mpp} is the maximum power point current, and I_{sc} is the short circuit current [6].

The I_{pv}–V_{pv} curve is affected by the variation of the solar irradiance (G) and temperature (T_α). The new characteristic curve $I_{pv,new}$–$V_{pv,new}$ then is represented by the following equations:

$$I_{scr} = \frac{I_{sc}}{(G/G_r)(1 + \alpha(T - T_r))} \quad (7)$$

$$\Delta T_\alpha = T_\alpha - T_r \quad (8)$$

$$\Delta I_{pv} = K_I\left(\frac{G}{G_r}\right)\Delta T_\alpha + \left(\frac{G}{G_r} - 1\right)I_{scr} \quad (9)$$

$$\Delta V_{pv} = -K_V \Delta T_\alpha - R_s \Delta I_{pv} \quad (10)$$

where G_r is the solar irradiance under reference conditions, K_I is the current temperature coefficient, K_V is the voltage temperature coefficient, α is the correction factor of temperature, T_r is the temperature, and I_{scr} is the short circuit current under reference conditions [6].

So, the new values of the PV generator's voltage and current are given by

$$V_{pv,new} = V_{pv} + \Delta V_{pv} \quad (11)$$

$$I_{pv,new} = I_{pv} + \Delta I_{pv} \quad (12)$$

Using ENRC, the non-linear diode is modelled as the parameter represented by the resistance g_{pv0} of the P–N junction. The parameter g_{pv0} can be expressed as

$$g_{pv0} = (I_{sc} K_1 K_2 m) V_{pv}^{m-1} e^{K_2 V_{pv}^m} \quad (13)$$

2.2 Proposed PV generator model validation

The PV module, here, composed by ($N_s = 54$) series-connected polycrystalline cells ($N_p = 1$). Table 1 shows the PV system model data [6]. The *I–V* characteristic of the proposed PV generator model is investigated by adding resistor–inductor–capacitor (RLC) equivalent circuit to the PV generator model. The data of both the PV generator and the RLC circuit is given in Table 1 [6].

The change of the PV generator output characteristic with the change of solar radiation and temperature is examined. First, the solar radiations are kept constant and equal to 1000 W/m^2 for different temperatures. Then, with a constant temperature, i.e. equal to 35°C, the solar radiations are kept constant. With different temperatures and solar radiations, the *I–V* and *P–V* output characteristics of the PV array are shown in Fig. 2.

2.3 Modelling of the investigated PV system

The PV generator model with a controller for maximum power point tracking (MPPT), filter, inverter model, and isolation transformer interface and the PV generation system with the AC grid are the main parts of the investigated PV generation system model.

2.3.1 Modelling of the PV generator model and MPPT controller: The TACS/ATP investigated PV generation system model is illustrated in Fig. 3*a*. The model shows the four main components of the PV generation system. The analytical representation of the ENRC of the PV generator has been mentioned in Section 2.1. Table 2 shows the PV generator model data [6].

For the PV generation units (PVGUs), the incremental conductance (IC) technique is used to simulate the MPPT controller proposed model [16]. Under changeful atmospheric conditions, the IC technique offers steady performance [17, 18].

The main idea is to compare the IC ($(\Delta I_{pv})/(\Delta V_{pv})$) to the instantaneous conductance (I_{pv}/V_{pv}). Depending on the result, the panel changes its operating voltage, either increasing or decreasing

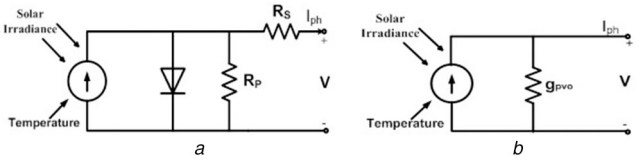

Fig. 1 *PV Cell equivalent circuit*
(a) Single-diode model [4], ***(b)*** ENRC model

Table 1 PV system model data

PV generator model data			
*P_{pv} = 110 W	V_{oc} = 43.5 V	T_α = 35°C	N_p = 1
*P_{mpp} = 110 W	I_{sc} = 3.45 A	T_r = 25°C	N_s = 54
V_{mpp} = 35 V	G = 900 W/m^2	α = 0.00085	K_I = 0.0014 A/°C
I_{mpp} = 3.15 A	G_r = 1000 W/m^2	R_s = 0.0221 Ω	K_V = − 0.152 V/°C

RLC equivalent circuit data			
$\delta t = 1 \times 10^{-5}$ s	C = 100 μF	L = 10 mH	R = 122.592 Ω

*P_{pv}: PV cell power; *P_{mpp}: maximum power point voltage.

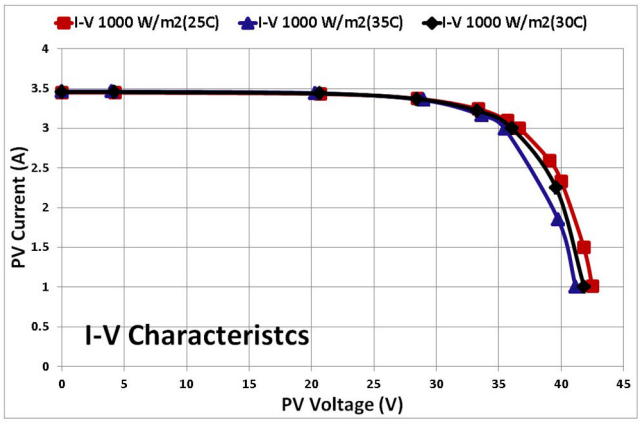

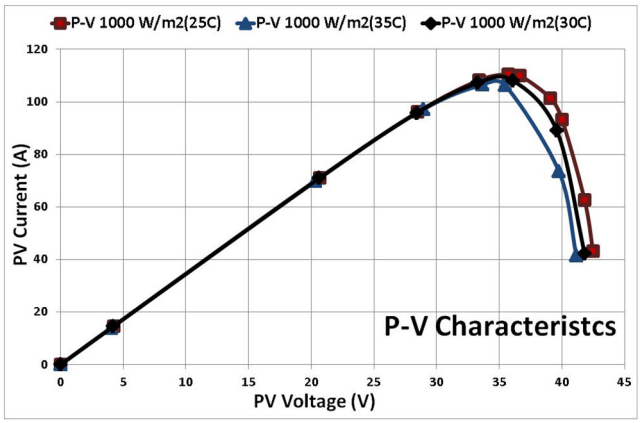

a

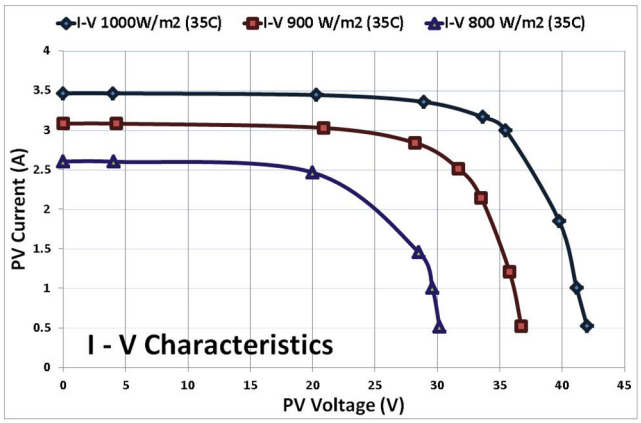

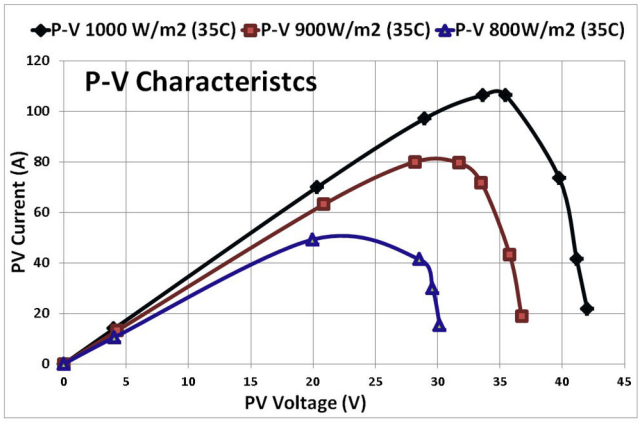

b

Fig. 2 *PV characteristics for*
(a) Different cell temperature, ***(b)*** Different solar irradiance

the operating voltage, until the maximum power point is reached. The MPPT controller ATP/EMTP model is illustrated in Fig. 3*b*.

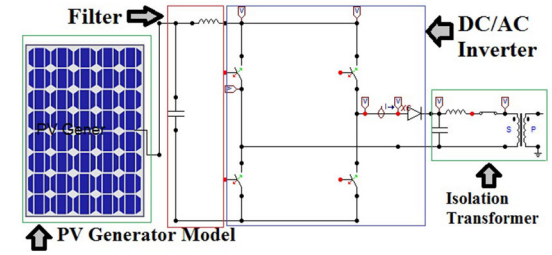

a

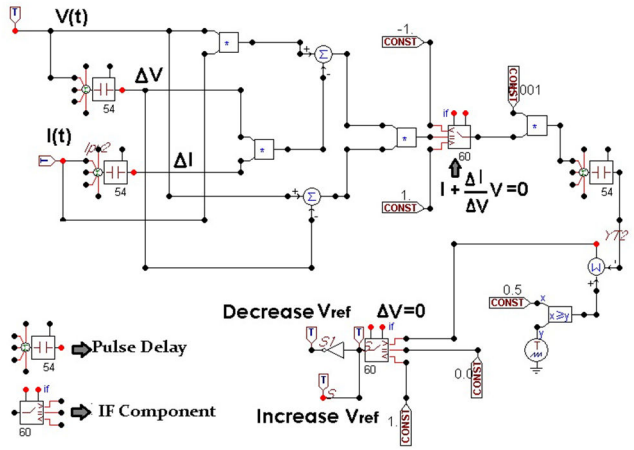

b

Fig. 3 *ATP model of*
(a) PV system, ***(b)*** IC/MPPT

Table 2 PV generator model data

V_{mpp} = 158 V	V_{oc} = 197 V	G = 1000 W/m^2
I_{mpp} = 15 A	I_{sc} = 17 A	T_α = 35°C

2.3.2 Modelling of the filter: The inductor–capacitor filter is designed to reduce and smooth high-order DC harmonics introduced by the DC/AC inverter and to limit the rate of change of DC generated by the PV generator.

2.3.3 Modelling of the inverter: A DC/AC inverter is connecting the PV generator model with the AC grid to modulate the generated power (DC) into the utility grid (AC). Two pairs of thyristors are represented the DC/AC inverter, as shown in Fig. 3*a*.

The ATP/EMTP inverter model uses the TACS-controlled TYPE 13 switches to represent the thyristors. The inverter model measures the voltage difference across the thyristors and sent it as input to the MPPT controller, which will give the firing signals as output and by that control the TACS thyristors [16].

2.3.4 Modelling of the isolation transformer: The isolation transformer used is an ideal TYPE 18 transformer with unit ratio and includes only an equivalent inductance for both primary and secondary sides [16].

3 The PV system model validation for switching studies

The utilisation of the PV system model for switching studies is investigated using two different electrical systems. The first one is a single-phase electrical system and the second is a three-phase electrical system.

3.1 The PV system model validation using single-phase electrical system

For the PV system validation for switching studies, a 240 V single-phase electrical power system is added to the PV generation system

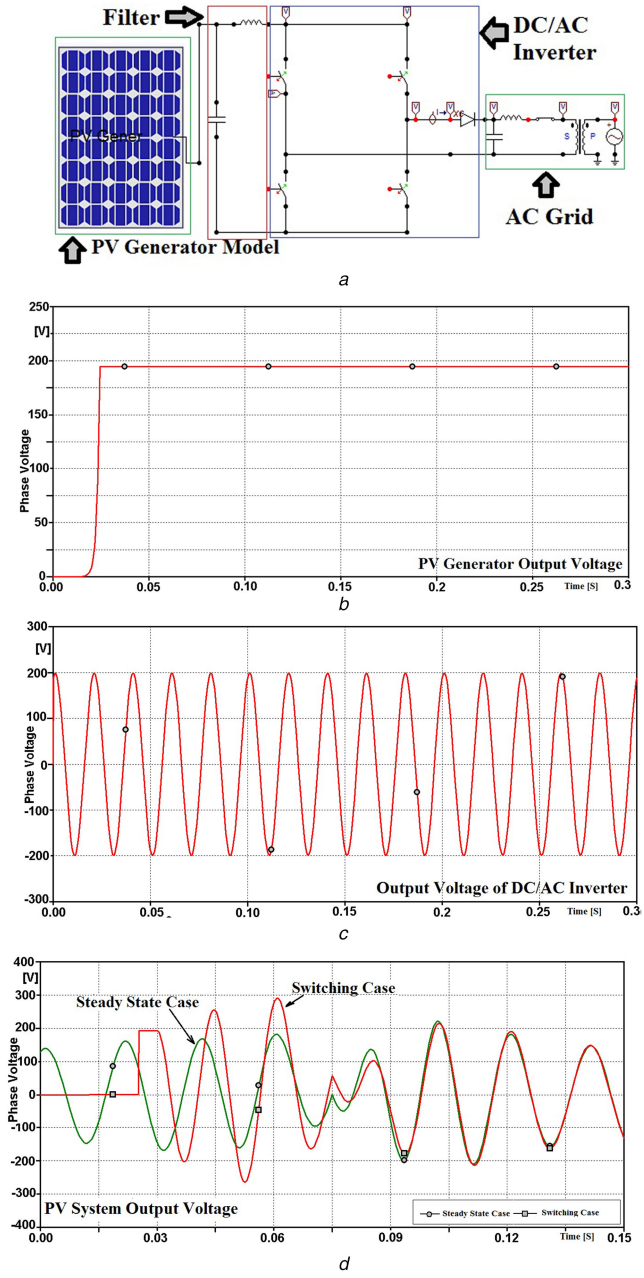

Fig. 4 *Investigated single-phase PV generation system*
(a) ATP/EMTP model, ***(b)*** PV generator output voltage, ***(c)*** DC/AC inverter output voltage, ***(d)*** TOVs effect on the proposed PV system output voltage

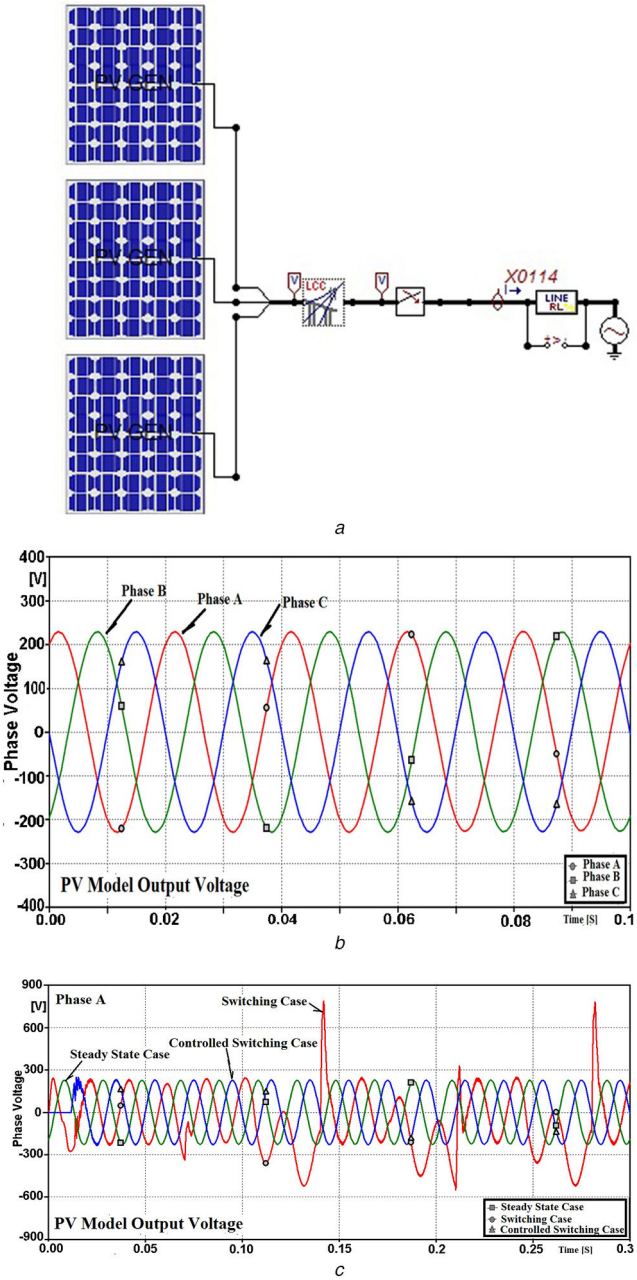

Fig. 5 *Investigated three-phase PV generation system*
(a) ATP/EMTP model, ***(b)*** PV system output voltage, ***(c)*** TOVs effect on PV system output voltage with and without the mitigation method

model. The TACS/ATP model for the tested electrical power system and the PV generation system model are shown in Fig. 4*a*.

The output voltages of the PV generation system model components are shown in Figs. 4*b* and *c*. It can be seen in Fig. 4*b* that the output of the PV generator took a period of time (<0.05 s) to settle at a fixed value, however, the output voltage is constant, which means that the PV generator works steadily and continuously. Fig. 4*c* shows the AC output voltage of the DC/AC inverter. Here, the inverter successfully turns the DC output of the PV generator into AC output voltage equals 200 V.

For the PV generator model validation for transient studies, an energisation operation is performed at the investigated system. Fig. 4*d* illustrates the TOVs effect on the output voltage of the proposed PV system.

When the energisation operation is applied, the switching causes the output voltage of the PV generator to increase to almost the double of its steady-state values. The PV system output voltage increase from 1.07 pu (169.66 V) to 1.835 pu (291.06 V).

3.2 The PV system model using three-phase electrical system validation

A three-phase system with an ideal three-phase 360 V AC voltage source is used, for this test, to represent the utility grid. The transmission system parameters are given in [19]. The TACS/ATP model of the tested three-phase PV generation system added to the PV generation system model is shown in Fig. 5*a*. Fig. 5*b* illustrates the steady-state AC output voltage of the PV generation system model.

For the PV generator model effectiveness for transient studies, an energisation operation is performed at the investigated system. A switching is carried out by the energisation of one of the transmission system circuit breakers. A controlled switching operation is performed at the switching point circuit breaker to mitigate TOVs.

Fig. 5*c* illustrates the TOVs effect on the output voltage of the proposed PV system with and without the mitigation method, respectively.

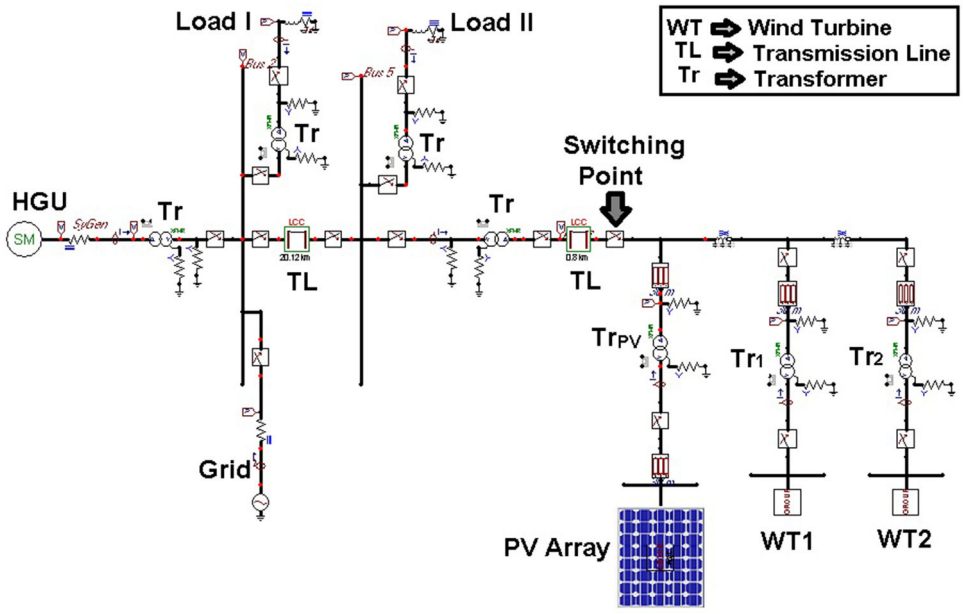

Fig. 6 *the ATP/EMTP model of the investigated μG including PVGU*

Table 3 Parameters of the distributed generation sources

DFIG-based WT	
stator resistance	0.0025 Ω
stator leakage inductance	0.097 mH
magnetization inductance	3 mH
rotor resistance	0.0383 Ω
rotor leakage inductance	0.115 mH
electrical turn ratio	4
moment of inertia (inertia constant = 2 s.)	2.400 kg m^2
rated apparent power	6.500 kVA

Synchronous generator-based HGU	
S_n = 5 MVA	x''_q = 0.17 pu
U_n = 6.6 kV	x_0 = 0.046 pu
R_A = 0.004 pu	T'_{d0} = 1.754 s
x_L = 0.1 pu	T'_{q0} = 0 s
x_d = 1.8 pu	T''_{d0} = 0.019 s
x_q = 1.793 pu	T'_{q0} = 0.164 s
x'_d = 0.166 pu	H = 74.8 kg m^2
x'_q = 0.98 pu	P = 4 poles
x''_d = 0.119 pu	ω_s = 188.5 rad/s

The PV model steady-state output voltage value is 228.62 V, whereas the switching is applied at the voltage peak, the maximum TOV is increased to 786.94 V (3.442 pu).

It can be seen that the use of controlled switching of circuit breaker reduces the TOVs at all phases A, B, and C of the output voltage of the proposed PV model.

4 Description and modelling of the μG system including PV arrays

4.1 The μG system general description

The μG system consists of three RDGR systems. The first system consists of a HGU connected to an 8 MVA, 6.9/66 kV power transformer, the hydro generation system is connected to bus 1. Wind power generator units (WPGUs), which consist of two WTs, represent the second RDGR system. The turbines are connected to a 5 MVA, 0.69/12.5 kV power transformer each. The third RDGR system is a PV generation system added nearby the WPGUs area. A 30 m transmission line TL_d is separated from the WTs from the PV array [20]. Two of the RDGR systems, WPGUs and PV generation system are connected to bus 7 through a 45 MVA, 12.5/66 kV power transformer and a 0.8 km transmission line TL_2. A 66 kV, 1000 MVA voltage source connected to bus 3 represented the utility grid. A 5 MVA, 66/12.5 kV power transformer is connected to Load_I and both are connected to bus 4. A 4 MVA, 66/12.5 kV power transformer is connected to Load_II and both are connected to bus 6. A 20.12 km transmission line TL1 connected the RDGR systems with the two loads. [21, 22]. Fig. 6 illustrated the ATP/EMTP model of the investigated μG test system.

4.2 Modelling of the RDGRs powered the μG system

The PV array is composed of (N_s* = 54) series-connected polycrystalline cells (N_p* = 31). Previously, the PV generator model data is illustrated in Section 2.3.

The two WTs are modelled using the ATP/EMTP WT model. The model consists of the wind speed, aerodynamic, and electrical components models. The ATP/EMTP model also includes a doubly-fed induction generator (DFIG), pulse width modulated converters, transformers, and the control and supervisory system [23].

The HGU is modelled using a synchronous generator [22, 24]. Table 3 briefs the data used to parameterise the two WTs and the HGU ATP/EMTP models, respectively.

4.3 Modelling of transformers and overhead lines

The μG transformers are modelled using a recommended model for transient studies. The ATP/EMTP hybrid transformer model is used to simulate the transformers at the μG system [25, 26].

Line/cable constant model, which is suitable for the electromagnetic transient studies, is used to simulate the medium-voltage overhead lines that connect between the two load areas and the generation units [27, 28]. Tables 4 and 5 give the data required for transformers and overhead lines modelling, respectively.

5 Description and modelling of the TOV mitigation methods

5.1 SVC-based TOV mitigation method

SVC is one of the most diffuse FACTS shunt devices [12, 13]. For this study, The SVC-based TOV mitigation method is considered. A SVC that consists of a thyristor controlled reactor (TCR) in

Table 4 μG's transformers data

Data	T1	T2	T3	T4	Twt
connection method	Y_Nd_{11}	Y_Nd_{11}	Y_Nd_{11}	Y_Nd_{11}	Y_Nd_{11}
voltage, kV	6.9/66	66/12.5	66/12.5	66/12.5	0.69/12.5
rated power, MVA	10	5	4	30	5
S.C Imp[a], %	9	8	8	9	5.7
copper losses, kW	24.75	32.4	28.8	126.9	1.58
no-load losses, kW	11.2	7.2	6.08	31.8	0.97

[a]S.C Imp: short circuit impedance.

Table 5 Parameters of the 12.5 kV transmission lines

Phase no.	1	2	3	0
R_{in}, cm	0.63	0.63	0.63	0
R_{out} ,cm	1.81	1.81	1.81	0.5
Resis, Ω/km	0.042	0.042	0.042	0.2
horiz, m	−2	0	2	0
Vtower, m	14	14	14	18
Vmid, m	11	11	11	15
separ, cm	40	40	40	0
alpha, deg	0	0	0	0

Table 6 Mitigation methods models data

SVC-based mitigation method model data			
parameters	L_r	C_f	R_d
values	34 mH	10 μF	100 Ω

Supercapacitor-based mitigation method model data				
parameters	C	R_S	R_E	L
values	6.9 μF	1.44 Ω	2.8 Ω	1.74 mH

parallel with a fixed capacitor is used. TCR is one of the most popular thyristor-based SVCs [29, 30].

Two antipolar thyristors represent the switching elements of the SVC model. The thyristors are conducted on alternate half cycles of the μG generation units' frequency [29, 30].

Owing to the non-continuity of the reactor current, thyristors controlled inductors are installed between phases in delta connection to guarantee the continuity of the TCR. A damping resistor is added, across the controlled inductors, to limit the problem of numerical oscillation [31].

The gate pulse generator (GPG), regulator, and root-mean-square (RMS) voltage detector are the three main parts of the control system of the TCR model. The thyristors firing pulses are supplied by the GPG. Meanwhile, the thyristors conduction angle is accounted for by the regulator, which is passed to the GPG as a control signal. Finally, the RMS voltage detector interfaces the TCR with the μG system. In this case, TCR measures the RMS voltage [30]. The parameter of the SVC model, for each phase, is given in Table 6.

5.2 Supercapacitor-based TOV mitigation method

Supercapacitors have time constants longer than the time duration of power line transients in the range of few microseconds to several hundred microseconds, therefore, supercapacitors could be used to withstand short duration surges [13–15].

Many equivalent circuits and models are introduced in the literature for supercapacitors [32, 33]. The parameters of the supercapacitor-based mitigation method include equivalent series resistance (R_S), small reactor (L), equivalent parallel resistance (R_P), and capacitance (C) [34, 35].

R_S represents the internal component of the supercapacitor [36, 37]. When charging or discharging the supercapacitors, the west internal heating power is determined by R_S. R_S is a small resistance (100–10 Ω), however, R_S impacts energy efficiency and power density [36, 38].

The small reactor (L) is added in series with the series resistances (R_S). The reactor is added to R_S, together, they formed a filter to minimise the harmonics in the waveform and make it smoother.

R_P is an inner equivalent parallel resistance usually in the order of several kilo-ohms and decides the leakage current when the supercapacitor is in a standby mode [36, 39].

In the supercapacitor model, a small capacitor is added in series with the classical supercapacitors capacitance C, and a small resistance is added, as a damping element, in parallel with R_P.

The parameters of the supercapacitor, in this study, are given in Table 6.

6 Mitigation of TOV in μG based on SVC and/or supercapacitor

The TOVs resulting from a faulty de-energisation operation on a μG system are investigated. The switching point located nearby the PV generation unit. The TOVs mitigation methods are located nearby the switching point circuit breaker.

The de-energisation is performed by an unsymmetrical switching of phases A and B, together, of the switching circuit breaker. These unsymmetrical switching operations are applied at a peak voltage of each phase, and thus the worst expected case of the de-energisation operation.

The uses of different mitigation methods for TOVs at the μG are investigated. Three different mitigation methods are considered. First, a reactive power compensation device such as SVC is represented as a TOVs mitigation method. Then, adding an energy storage device to the μG, such as a supercapacitor, as TOVs

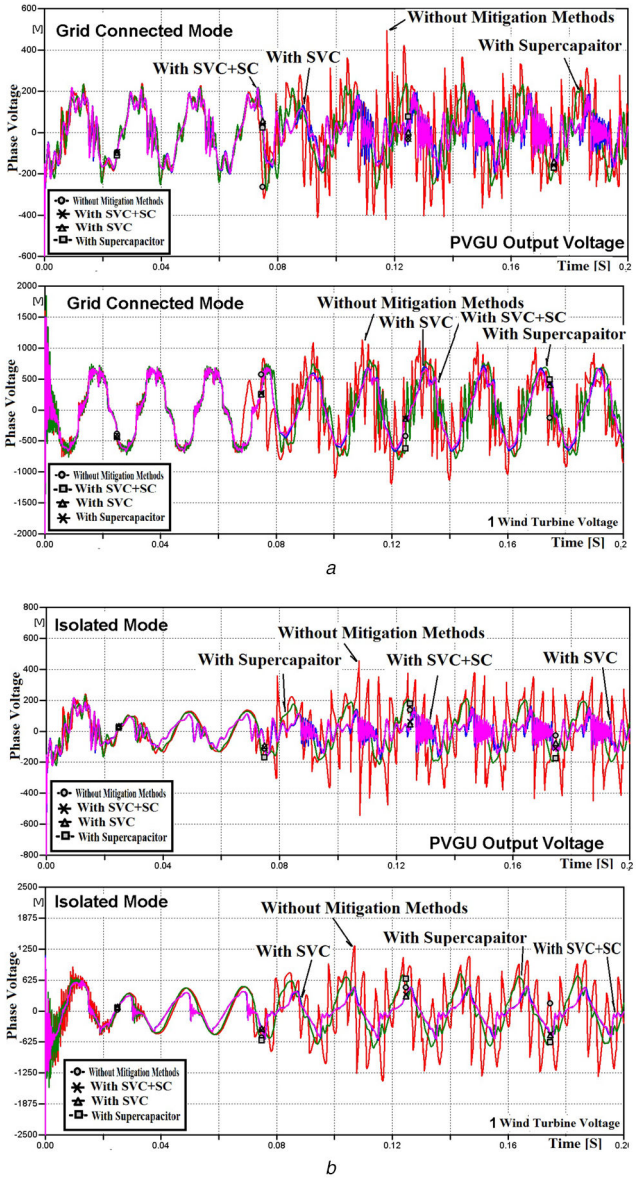

Fig. 7 *Maximum TOV with and without mitigation methods at PVGU and first WT output voltages, respectively*
(a) Grid-connected mode, ***(b)*** Isolated mode

mitigation method is evaluated. After that a combination of active and reactive power simultaneously to mitigate TOV, by the addition of SVC to the supercapacitor is investigated. The grid-connected mode and isolated mode of the μG are considered.

6.1 Grid-connected mode

In this subsection, the μG in grid-connected mode is tested when the SVC and/or the supercapacitor are installed. Figs. 7*a* and *b* show the maximum TOVs at RDGRs output voltage without/with the mitigation methods; the PV generation unit and the first WT, respectively.

AC power quality is a general term for indices that describe the impact on customer-device operation due to deviations from prescribed tolerances in the sinusoidal voltage's amplitude, frequency, phase, and waveform. From this point of view, it can be concluded that the switching operation affects AC power quality.

When the switching is applied at $t = 0.0665$ s with only two phases opens, the frequency of the PV generation unit is increased to reach 500 Hz ten times the normal frequency of the system. The switching operation causes the PV generation unit maximum output voltage to reach 457.2 V and exceed the impulse withstand voltage which equals 440 V.

Using the mitigation methods, individually or together, helps in reducing both the frequency and the magnitude of the switching overvoltage to a range close to its normal values. Comparing the results, adding the supercapacitor to the SVC achieved better results compared to the other two investigated mitigation methods. In addition, it can be noted that using the supercapacitor or using the supercapacitor with the SVC result in more regular voltage waveform comparing with using only the SVC. However, using the supercapacitor individually or adding the supercapacitor to the SVC results in a small shift in the phase angle.

When the switching is applied, the WTs output voltage frequency increases to reach 550 Hz 11 times the normal frequency of the system. The switching operation causes the first and the second WTs maximum output voltage to reach 1194.7 and 1205 V, respectively. These results exceed the maximum switching impulse overvoltage for the WTs, which equals 1000 V.

As a TOV mitigation method, adding the supercapacitor to the SVC achieved better results compared to the other two investigated mitigation methods. However, using the supercapacitor individually results in a more uniform voltage waveform comparing to the other two mitigation methods. The switching frequency is reduced to a range close to its normal values, due to the installation of the mitigation methods.

Table 7 summarised the maximum TOV at the output voltage of the RDGRs with and without mitigation methods at grid-connected mode.

6.2 Isolated mode

The tested μG is isolated from the grid when the SVC and/or the supercapacitor are installed. The μG is isolated from the grid at $t = 0.015$ s. Figs. 7*a* and *b* show the maximum TOVs at RDGRs output voltage without/with the mitigation methods; the PV generation unit and the first WT, respectively.

The isolation operation causes the PV generation unit output voltage to decrease to around 73% of its nominal voltage. However, at $t = 0.0665$ s, when the switching operation occurs PV generation unit output voltage increases to reach 544.5 V. The frequency of the PV generation unit is increased, due to the switching operation, to reach 300 Hz seven times the normal frequency of the system.

It can be noticed that at the PV generation unit, as a TOV mitigation method, adding the supercapacitor to the SVC achieved better results compared to the other two investigated mitigation methods. Using the supercapacitor or using the supercapacitor with the SVC results in a more uniform voltage waveform comparing to using the SVC. Using the mitigation methods helps in reducing the frequency to a range close to its normal values. However, using the supercapacitor or adding the supercapacitor to the SVC results in a small shift in the phase angle.

Owing to the isolation operation, the first and second WT output voltage decrease to around 73 and 77% of its nominal voltage, respectively. The switching operation causes the first and second WT output voltage to increase to reach 1414.1 V for both turbines. Also, due to the switching operation, the switching frequency increases to reach 250 Hz five times the normal frequency of the system.

As the results show at WTs, as a TOV mitigation method, the supercapacitor added to SVC achieved better results compared to the other two investigated mitigation methods. However, using the supercapacitor individually results in a more uniform voltage waveform and more acceptable results comparing with the other two mitigation methods. Owing to the installation of the mitigation methods, the switching frequency is reduced to a range close to its normal values. However, using the supercapacitor or adding the supercapacitor to the SVC results in a small shift in the phase angle.

Table 7 summarised the maximum TOV at the output voltage of the RDGRs with and without mitigation methods at isolated mode.

Comparing the tested μG with the μG previously tested in [20] that does not include PV arrays, the μG powered with only WT generators (WTGs) has higher transient overvoltage level. Since the WTGs are designed to operate at high power level unlike the PV systems electronics. However, PV systems are commonly used

Table 7 Output voltage of the RDGRs with and without mitigation methods at grid connected mode and isolated mode

Grid-connected mode								
State	Without mitigation methods		SVC		SC		SVC + SC	
Unit	P.U.	V	P.U.	V	P.U.	V	P.U.	V
PVGU	2.32	457.2	1.12	219.6	1.21	238.8	0.97	191.7
1st WT	1.73	1194.7	0.95	658.4	1.16	798.9	0.97	670.2
2nd WT	1.75	1205	0.98	674.8	1.02	702.2	0.93	639.1
HGU	1.07	7053.9	0.98	6462	1.02	6708	0.98	6461.8

Isolated mode								
State	Without mitigation methods		SVC		Supercapacitor (SC)		SVC + SC	
Unit	P.U.	V	P.U.	V	P.U.	V	P.U.	V
PVGU	2.76	544.5	0.9	176.5	1.08	211.8	0.82	160.7
1st WT	2.05	1414.1	0.87	599.7	1.06	730.2	0.82	562.9
2nd WT	2.05	1414.1	0.85	588.1	1.09	749.1	0.82	562.9
HGU	1.04	6850	1.02	6731	1.03	6786.6	1.02	6735

RDGRs and much more convenient in urban and suburban environments such as μGs.

7 Conclusion

This study investigates the mitigation of transient TOVs in a μG supplied by RDGRs, which includes PV generators, HGU, and WPGs. ATP is used in this study as electromagnetic transient software. Accurate simulation models are needed to carry out the study. Therefore, a three-phase PV system model based on ENRC is used.

The model *I–V* and *P–V* output characteristic curves show a perfect response to the change in solar radiation and temperature. The use of the proposed PV system model in switching studies is evaluated using two different electrical systems. During all the tests, with the different connected systems, the proposed PV system model works steadily and continuously.

The effectiveness of using different TOV mitigation methods such as SVC and/or the supercapacitor is evaluated. The investigated μG including PV arrays as a power source. The μG two operational modes, grid-connected mode and isolated mode, are considered.

At the RDGRs output voltage, the results show that in the μG two operational modes, adding the SVC to the supercapacitor achieved better results compared to the other two investigated mitigation methods. However, using the SC individually or adding the SVC to the supercapacitor, results in more uniform voltage waveform compared to using the SVC only.

8 References

[1] Xavier, G., Filho, D., Martins, J., *et al.*: 'Simulation of distributed generation with photovoltaic microgrids—case study in Brazil', *Energies J.*, 2015, **8**, pp. 4003–4023

[2] Khalil, A., Ateea, K.: 'Modelling and control of photovoltaic-based microgrid', *Int. J. Renew. Energy Res.*, 2015, **5**, (3), Pp. pp. 1–10

[3] Benkhelil, E., Gherbi, A.: 'Modeling and simulation of grid-connected photovoltaic generation system'. Renewable Energies and Vehicular Technology Conf., REVET, Hammamet, Tunisia, 26–28 March 2012, pp. 295–306

[4] Theocharis, A., Charalampakos, V., Drosopoulos, A., *et al.*: 'Equivalent circuit of photovoltaic generator using Newton–Raphson algorithm', *Int. J. Comput. Math. Electr. Electron. Eng.*, 2012, **31**, (4)

[5] Fuchs, E., Masoum, M.: 'Power quality in power systems and electrical machines', 2008. Available at http://www.sciencedirect.com

[6] Breza, P.: 'Modelling and simulation of a PV generator for applications on distributed generation systems'. MSc thesis, Delft University, The Netherlands, November 2013

[7] Cho, H., Yeo, S., Kim, C., *et al.*: 'A steady-state model of the photovoltaic system in EMTP'. Int. Conf. on Power Systems Transients, IPST'09, Kyoto, Japan, 3–6 June 2009

[8] dos Santos, C., de Almeida, J., Davi, M., *et al.*: 'A contribution of a computer tool using ATP-EMTP TACS to the modeling of a photovoltaic (PV) module'. Int. Conf. on Renewable Energies and Power Quality, ICREPQ'15, La Coruña, Spain, 25–27 March 2015, pp. 300–305

[9] Karimi, S., Farjah, E., Ghanbari, T.: 'Common and differential modes of conducted electromagnetic interference in electric vehicle equipped with supercapacitor'. 10th Int. Power Electronics, Drive Systems and Technologies Conf., PEDSTC, Iran, 12–14 February 2019

[10] Wang, L., Lam, C., Wong, M.: 'Minimizing inverter capacity design and comparative performance evaluation of SVC-coupling hybrid active power filters', *IEEE Trans. Power Electron.*, 2019, **34**, (2), pp. 1227–1242

[11] Shah, G., kash, A., Saxena, N.: 'Systematic survey for role of reactive power compensating devices in power system', *Int. J. Electr. Instrum. Eng.*, 2013, **3**, (2), pp. 89–94

[12] Akwukwaegbu, I.O., Gerald, I.O.: 'Concepts of reactive power control and voltage stability methods in power system network', *Int. Org. Sci. Res. J. Comput. Eng., IOSR-JCE*, 2013, **11**, (2), pp. 15–25

[13] Kakimoto, N., Satoh, H., Takayama, S., *et al.*: 'Ramp-rate control of photovoltaic generator with electric double-layer capacitor', *IEEE Trans. Energy Convers.*, 2009, **24**, (2), pp. 465–473

[14] Zarghami, M., Crow, M.L., Sarangapani, J., *et al.*: 'A novel approach to inter-area oscillation damping by unified power flow controllers utilizing ultracapacitors', *IEEE Trans. Power Syst.*, 2010, **25**, (1), pp. 404–412

[15] Kularatna, N., Fernando, J., Pandey, A.: 'Surge endurance capability testing of supercapacitor families'. IEEE Industrial Electronics Society Conf., IECON 2010, Glendale, USA, November 2010, pp. 1858–1863

[16] Awad, E.A., Badran, E.A.: 'A proposed ATP/TACS-based PV generator model'. 20th Int. Middle East Power Systems Conf., MEPCON'18, Cairo, Egypt, 18–20 December 2018, Paper No. 54

[17] Beriber, D., Talha, A.: 'MPPT techniques for PV systems'. 4th Int. Conf. on Power Engineering, Energy and Electrical Drives, POWERENG, Istanbul, Turkey, 13–17 May 2013

[18] Tey, K., Mekhilef, S.: 'A fast-converging MPPT technique for photovoltaic system under fast varying solar irradiation and load resistance', *IEEE Trans. Ind. Inf.*, 2015, **11**, (1), Pp. pp. 176–186

[19] Soloot, A., Gholami, A., Agheb, E., *et al.*: 'Investigation of transmission line overvoltages and their deduction approach', *World. Acad. Sci. Eng. Technol.*, 2009, **53**

[20] Awad, E.A., Badran, E.A., Youssef, F.H.: 'Mitigation of switching overvoltages in microgrids based on SVC and supercapacitor', *IET Gener. Transm. Distrib. J.*, 2018, **12**, (2), pp. 355–362

[21] Kumar, M., Reddy, M.: 'Renewable power generation units through micro grid system', *Int. J. Eng. Res. Appl.*, 2013, **3**, (5), pp. 1559–1563

[22] Ahshan, R., Iqbal, M., Mann, G., *et al.*: 'Modeling and analysis of a microgrid system powered by renewable energy sources', *Open Renew. Energy J.*, 2013, **6**, pp. 7–22

[23] La Seta, P.: 'Modeling and control of wind turbines based on doubly-fed induction generators (DFIG)'. EEUG Meeting 2009, TU Delft, the Netherlands, 2009

[24] Moura, F., Camacho, J., Resende, J., *et al.*: 'Synchronous generator, excitation and speed governor modeling in ATP-EMTP for interconnected DG studies'. Int. Conf. on Electrical Machines, ICEM'08, Vilamoura, Portugal, 2008

[25] Chiesa, N., Høidalen, H.K., Mork, B., *et al.*: 'Implementation and verification of the hybrid transformer model in ATPDraw'. Int. Conf. on Power Systems Transients, IPST'07, Lyon, France, 4–7 June 2007

[26] Hassan, E.O., Badran, E.A., Youssef, F.M.H.: 'A comparison between some currently used high frequency transformer models', *Mansoura Eng. J.*, 2013, **39**, (1), pp. E1–E7

[27] Prikler, L., Høidalen, H.: 'ATPDRAW version 5.6 users' manual', November 2009

[28] Ali, S.A.: 'Study of short-circuit currents around detmarovice power station', *Trans. Electr. Electron. Mater.*, 2014, **15**, (3), pp. 117–124

[29] Khonde, S., Palandurkar, M.: 'Simulation model of thyristor controlled reactor', *Int. J. Eng. Res. Technol.*, 2014, **3**, (4), pp. 1692–1694

[30] 'TCR Modeling Using ATP', EPRI Report, 1995

[31] Mahapatra, S., Goyal, A., Kapil, N.: 'Thyristor controlled reactor for power factor improvement', *Int. J. Eng. Res. Appl.*, 2014, **4**, (4), pp. 55–59

[32] Spyker, R.L., Nelms, R.M.: 'Classical equivalent circuit parameters for a double-layer capacitor', *IEEE Trans. Aerosp. Electron. Syst.*, 2000, **30**, (3), pp. 829–836
[33] Hajizadeh, A., Golkar, M.A., Norum, L.: 'Robust control of hybrid fuel cell/energy storage distributed power generation system in weak grid under balanced and unbalanced voltage sag', *Eur. Trans. Electr. Power*, 2011, **21**, (1), pp. 522–540
[34] Awad, E.A., Badran, E.A., Youssef, F.H.: 'A proposed supercapacitor-based mitigation of microgrid switching overvoltage', *Int. Trans. Electr. Energy Syst. J.*, 2018, **28**, (2), pp. 1–17
[35] Awad, E.A., Badran, E.A., Youssef, F.H.: 'Mitigation of microgrid's switching overvoltages using supercapacitor'. 19th Int. Middle East Power Systems Conf., Menoufia, Egypt, 19–21 December 2017, Paper No. 104
[36] Sahay, K., Dwivedi, B.: 'Design and analysis of supercapacitor energy storage system for energy stabilization of distribution network', *Electr. Power Qual. Utilisation*, 2009, **15**, (1), pp. 25–32
[37] Halper, M.S., Ellenbogen, J.C.: 'Supercapacitors: a brief overview', MITRE Nano-systems Group, March 2006. Available at http://www.mitre.org
[38] Kularatna, N., Fernando, J., Pandey, A., *et al.*: 'Surge capability testing of supercapacitor families using a lightning surge simulator', *IEEE Trans. Ind. Electron.*, 2011, **58**, (10), pp. 4942–4949
[39] James, S., Kularatna, N., Ross, A., *et al.*: 'Estimation of transient surgy energy transferred with associated time delays for individual components of surge protector circuits', *Inst. Eng. Technol., IET Power Electron. J.*, 2015, **8**, (5), pp. 685–692

9 Appendix

9.1 SVC-based TOV mitigation method

The inductor (L_r) which is connected in series with the thyristors, in the TCR, is given by

$$\frac{1}{L_r} = \frac{\omega P}{V_{rms}^2}\left(\frac{P}{Q} + \frac{Q}{P}\right) \tag{14}$$

where ω is the angular frequency, P is the rated TCR active power, V_{rms}^2 is the RMS voltage of the TCR, and Q is the rated TCR reactive power.

The capacitive reactance (X_C) of the fixed capacitor (C_f) connected in parallel with the TCR is given by

$$X_C = \frac{V_{rms}^2}{Q} \tag{15}$$

A damping resistor (R_d) is introduced, in this study, across the inductor (L_r) to stop the problem of numerical oscillation. This resistor is represented as

$$R_d = \frac{L_r}{\beta\ \Delta t} \tag{16}$$

where β is a damping factor of the reactor, $0 \leq \beta \leq 1$, and Δt is the time step of the simulation.

9.2 SC-based TOV mitigation method

The equivalent series resistance (R_S) is given by

$$R_S = \frac{V_C^2}{4 \times P_{max}} \tag{17}$$

where R_S is the equivalent series resistance of the SC bank in ohm, V_C is the maximum voltage of the SC bank in volts, and P_{max} is the maximum dischargeable power in VA.

R, an equivalent resistance results from adding a resistance R_E in parallel with R_P. The equivalent resistance R_E is defined by

$$R_E = \frac{V_c}{I_D} \tag{18}$$

The capacitance C of the proposed SC-based mitigation method in μF can be expressed on the assumption that, if a single-step voltage of V_{max} in volts and time duration of T in seconds is applied to the SC, approximate final voltage developed at the capacitor is given by

$$V_c = \frac{T}{R_S \times C}\ V_{max} \tag{19}$$

Equations (6) and (19) provide that the surge duration T is very much shorter than the time constant of the circuit $T = R_S C$.